J Mater Sci (2008) 43:2935–2946
DOI 10.1007/s10853-007-1794-4

The electronic band structure of InN, InAs and InSb compounds

Rezek Mohammad · Şenay Katırcıoğlu · Musa El-Hasan

Received: 20 October 2006 / Accepted: 23 April 2007 / Published online: 3 July 2007
© Springer Science+Business Media, LLC 2007

Abstract The electronic band structure of InN, InAs and InSb has been investigated by ETB. The ETB method has been formulated for sp^3d^2 basis and nearest neighbor interactions of the compounds and its energy parameters have been derived from the results of the present first principles calculations carried on InN, InAs and InSb. It has been found that the present ETB parameters can produce the band structure of the compounds successfully.

Introduction

There is currently considerable interest in compounds of In with Nitrogen, Arsenic and Antimony, because of their optical and high temperature device applications. Among these compounds, InN is a highly potential material for the fabrication of high speed heterojunction transistors [1] and low cost solar cells with high efficiency [2]. Pure InN was predicted to have the lowest effective mass for electrons in all the III-nitride semiconductors [1] which lead to high mobility and high saturation velocity. Recently, several groups have grown high quality hexagonal (w-InN) and zinc-blende (c-InN) structural InN films by modern growth techniques, such as metal organic chemical vapor deposition (MOVPE) and plasma-assisted molecular beam epitaxy (MBE) [3–8]. The w-InN and c-InN films have been mostly grown on sapphire and GaAs (or Si, GaP) substrates, respectively. In these works [3–7], a buffer layer, particularly, AlN or InAs has been usually grown on the substrate to improve the quality of the InN films. In a very recent work [8], the c-InN has been grown on r-plane sapphire successfully without the use of additional buffer layer. The growth of w-InN and c-InN films have been characterized by many techniques such as, X-ray diffraction, Raman spectra, reflection high-energy electron diffraction (RHEED). The photoluminescence (PL) spectra of high quality w-InN films have illustrated that the band gap energy of InN is smaller than the commonly accepted value of 1.9 eV [9]; it is a round 0.65–0.90 eV [3, 4]. The recent experiment works on c-InN have mainly focused on the characterization of the films [5–8]. The band gap energy of c-InN films has not been reported experimentally, but it has been found around 0.44–0.74 eV by the results of ab-initio calculations [10, 11]. These newly reported values of w-InN and c-InN are compatible with the wavelength of the optical fiber. Therefore, the w-InN and c-InN films will have very important potential to fabricate high speed laser diodes (LDs) and photodiodes (PDs) in the optical communication system.

The other two compounds of In, InAs and InSb are interesting narrow gap semiconductors from the point of view of optical spectroscopy and optoelectronic applications [12]. Since InAs has a high electron mobility it may prove an important material for use in high speed electronics [13, 14]. The high quality InAs material has been grown with certain advantages by different growth techniques such as liquid phase epitaxy (LPE) [15], MBE [15–18], and MOCVD [15, 19]. The quality of grown doped [15] and undoped [15–19] InAs materials has been appraised by mainly PL spectroscopy [15–23] at different

R. Mohammad · Ş. Katırcıoğlu (✉)
Department of Physics, Middle East Technical University, Ankara 06531, Turkey
e-mail: senay@metu.edu.tr

M. El-Hasan
Department of Physics, An Najah University, West Bank, Palestine

temperatures. In the works on undoped homoepitaxial InAs (i.e. InAs/InAs), the energy of the first PL peak which corresponds to the band gap of InAs has been reported in the range of 399–418 meV at low temperatures ($T = 4.2$–10 K). The band gap of undoped heteroepitaxial InAs has been measured to be 416 and 399 meV at 4.6 K for the GaAs and Si substrates, respectively [16]. In Ref. [19], the energy of the first infrared-PL peak has been reported as 415 meV at 10 K. In an early work, Dixon and Ellis [24] measured the band gap of InAs as 420 meV at 18 K by transmission experiment. In another early work given in Ref. [25], the band gap of InAs is measured to be 0.41 eV at 0 K by direct interband magneto-optical transitions. The calculated band gap value of InAs by first principles [26] and empirical [27–33] methods are all in the rage of 0.37–0.42 eV.

The other compound of In, InSb, calls attention to have the smallest energy gap of any of the binary III–V materials. This property often allows the fabrication of infrared imaging systems, free space communications, and gas phase detection systems [34, 35]. There are many reports on the growth of InSb by MBE [36] and MOCVD [19] techniques. In a recent work [37], good quality InSb has been also grown by LPE technique. GaAs, Si and InSb (bulk like) have been mostly used substrates in all growth works. The possible lattice-mismatching between InSb and substrate in heteroepitaxial growths has been tried to be removed by the growth of buffer layers such as InSb and AlSb [36] on the substrate. The quality of grown homoepitaxial InSb (InSb/InSb) materials has been analyzed by mainly PL [19] and infrared spectra [37] measured at different temperatures. In Ref. [19] the energy of the first PL peak which corresponds to the band gap of InSb has been reported as 235 meV at 10 K. At the same temperature, the energy gap of InSb corresponds to infrared spectra has been measured to be 0.23 eV [37]. In Ref. [23], the direct band gap of InSb was given as 0.235 and 0.23 eV at 1.8 and 77 K, respectively. Rowell [38] measured the band gap value of InSb as 235 meV by infrared-PL at 5.1 K. In an early work given in Ref. [25], the band gap of InSb measured to be 0.24 eV at 0 K by direct interband magneto-optical transitions. In their experimental works, Littler and co-workers [39] measured the band gap energy of InSb as 0.2352 eV. In a very recent work [40], the direct band gap of InSb has been measured to be 0.18 eV. In the literature, the band gap of InSb has been calculated to be in the range of 0.18–0.26 eV by self-consistent pseudopotential (PP) [41], nonlocal PP [27], empirical tight binding [28, 31], empirical pseudopotential (EPP) [29], relativistic self-consistent linear muffin tin orbitals (LMTO) [42], density functional theory-local density approximation (DFT-LDA) [26, 43] and DFT-generalized Khon Sham scheme [44] methods.

In the present work, the electronic band structure of InN, InAs and InSb has been calculated by empirical tight binding (ETB) method. The aim of this work is to derive the energy parameters of ETB by minimal sp^3d^2 basis, providing well defined valence bands and energy gaps for InN, InAs and InSb. Therefore these energy parameters can be used for the electronic band structure calculations of large sized systems, such as the alloys of these compounds by consuming the computational time. The paper is organized as follows: in ''The electronic structure calculations'' section, we give a brief description for the calculational methods and the calculational steps of the ETB energy parameters. In ''The results'' secion, we report the results of the calculations for volume optimization and band structure of compounds considered in this work. The conclusion of the work is introduced in the ''Conclusion'' section.

The electronic structure calculations

At the first stage of the present work, we have considered the zinc-blende phase (cubic phase) of InN, InAs and InSb and performed electronic structure calculations based on DFT by means of the ab-initio full potential linearized augmented plane wave (FP-LAPW) method given in WIEN2k package [45]. The exchange correlation energy of electrons is described in gradient generalized density approximation (GGDA) based on Perdew and Wang functional [46]. Basis functions are expanded in combinations of spherical harmonic functions inside nonoverlapping spheres surrounding the atomic sites (muffin-tin (MT) spheres) and in a Fourier series in the interstitial region. Inside the MT spheres, the angular momentum expansion is truncated at $l = (12)$ for the wave function of InN, InAs and InSb compounds. In the calculations, the generated LAPW basis functions are approximately 1,240, 2,300 and 2,799 for InN, InAs and InSb, respectively. The value of $R_{mt}K_{max}$ is taken to be 8–12 (where K_{max} is the maximum modulus for the reciprocal lattice vector, and R_{mt} is the average radius of the MT spheres). (1000) Number of k points in the irreducible wedge of the Brillouin zone (BZ) have been used and the iteration process has been repeated until the calculated total energy of the considered compound converged to less than 0.1 mRy.

In the second stage of the work, we have employed ETB [47, 48] method in electronic band structure calculations of InN, InAs and InSb compounds. The ETB method has been received considerable attention because of its intuitive simplicity and its realistic description of structural and dielectric properties in terms of chemical bonds. Slater–Koster model of ETB was extensively used with minimal sp^3 basis and interaction only between nearest neighbor

atoms to find out valence band energy dispersion of compounds correctly. But this model fails to calculate the indirect gap of semiconductors satisfactorily, especially at X point. This deficiency was tried to be overcome by including an excited s state, s*, to the interactions in Vogl's ETB model [49]. On the other hand, the successfully reproduced indirect energy gaps of III–V compounds by pseudopotential method [50] and ETB [31, 32] showed that, the influence of the d orbitals to the lowest conduction state is large at Γ, X and L points. By considering this fact, in the present nearest neighbor ETB calculations, the excited first and second d orbitals, d_1 (d_{z^2}) and d_2 ($d_{x^2-y^2}$) are taken into account as well as sp^3. Since all the orbitals in sp^3d^2 set have the same symmetry group, the first nearest neighbor interactions between anion and cation can be defined by only thirteen different types of ETB energy parameters. They are E_{sa}, E_{pa}, E_{da}, E_{sc}, E_{pc}, E_{dc}, V_{ss}, V_{xx}, V_{xy}, V_{scpa}, V_{sapc}, V_{dapc}, V_{dcpa}. Here, the d–d and s–d orbital interaction energies (V_{dd} and V_{sd}) between the cation and the anion are considered to be small and neglected. In ETB calculations of compounds, the solution of the secular equation at Γ and X symmetry points gives nine independent equations:

$$E_{sc} = \Gamma_1^c + \Gamma_1^v + E_{sa} \quad (1)$$

$$E_{pc} = \Gamma_{15}^c + \Gamma_{15}^v + E_{pa} \quad (2)$$

$$V_{ss} = -\sqrt{\left(\frac{\Gamma_1^c - \Gamma_1^v}{2}\right)^2 - \left(\frac{E_{sa} - E_{sc}}{2}\right)^2} \quad (3)$$

$$V_{xx} = \sqrt{\left(\frac{\Gamma_{15}^c - \Gamma_{15}^v}{2}\right)^2 - \left(\frac{E_{pa} - E_{pc}}{2}\right)^2} \quad (4)$$

$$V_{xy} = \sqrt{\left(\frac{X_5^c - X_5^v}{2}\right)^2 - \left(\frac{E_{pa} - E_{pc}}{2}\right)^2} \quad (5)$$

$$V_{pcsa} = \sqrt{\left(\frac{(E_{sa} - X_1^c)(E_{sa} - X_1^v)(E_{pc} + E_{da} - X_1^v - X_1^c)}{(E_{sa} - E_{da})}\right)} \quad (6)$$

$$V_{pasc} = \sqrt{\left(\frac{(E_{sc} - X_3^c)(E_{sc} - X_3^v)(E_{pa} + E_{dc} - X_3^v - X_3^c)}{(E_{sc} - E_{dc})}\right)} \quad (7)$$

$$V_{dapc} = \sqrt{\frac{3}{4}\left(\frac{(E_{da} - X_1^c)(E_{da} - X_1^v)(E_{pc} + E_{sa} - X_1^v - X_1^c)}{(E_{da} - E_{sa})}\right)} \quad (8)$$

$$V_{dcpa} = \sqrt{34\left(\frac{(E_{dc} - X_3^c)(E_{dc} - X_3^v)(E_{pa} + E_{sc} - X_3^v - X_3^c)}{(E_{dc} - E_{sc})}\right)} \quad (9)$$

The interaction energy parameters of ETB have been derived from the eigenvalues of FP-LAPW studied for the compounds at the first stage of the work. The above equations have been solved for each compound by a simulating program which also finds the remaining four energy parameters (E_{sa}, E_{pa}, E_{da}, E_{dc}) by minimizing the difference between the eigenvalues of ETB and FP-LAWP. The ETB energy parameters of sp^3d^2 for InN, InAs and InSb in zinc-blende phase are listed in Table 1.

The results

InN

The zinc-blende structure of InN is characterized by the lattice constant, a. At the first stage of the work, the equilibrium value of a is determined by calculating total energy of InN by FP-LAPW for a set of volumes and fitting these to the Murnaghan equation [51]. We have adopted the value of 0.95 Å for In and 0.87 Å for N as the MT radii. The electronic configuration of InN is In:Kr ($4d^{10}5s^25p^1$) and N:He ($2s^22p^3$). In the calculations, the electrons of In in ($1s^22s^22p^63s^23p^63d^{10}4s^24p^64d^{10}$) are defined as the core electrons and distinguished from the valence electrons of In in ($5s^25p^1$). Similarly, the inner shell electrons of N in ($1s^2$) are distinguished from the valence band electrons of N in ($2s^22p^3$) shell. The curve of the total energy versus the lattice constant is shown in Fig. 1. The equilibrium lattice constant of c-InN is calculated to be 4.967 Å. The present lattice constant of c-InN is given in Table 2 together with the experimental and other calculated lattice constant values of c-InN presented in the literature. The present lattice constant of c-InN (4.967 Å) is found to be very close to the experimental result of 4.97 Å [5]; it is only 0.3% smaller than the other experimental results 4.98 Å [66] and 4.986 Å [8]. On the other hand, our lattice constant is also close to the lattice constant values of 4.968 Å [65], 4.964 Å [64], 5.017 Å [11], and 5.004 Å [57] calculated by DFT-Local Density Approximation (LDA).

The present lattice constant is approximately 0.34% greater than the other value of 4.95 Å calculated by (LMTO)[52], and pseudopotential plane wave (PPPW)-GG approximation [10, 53]. Another lattice constant value of 5.067 Å [64] calculated by DFT within GGA is greater than the present value by 2%. The present lattice constant

Table 1 Empirical matrix elements of the sp^3d^2 Hamiltonian in eV

	InN	InAs	InSb
E_{sa}	–11.6558	–7.9244	–5.5942
E_{sc}	–2.6424	–2.8927	–3.2074
E_{pa}	4.6235	0.0000	0.0000
E_{pc}	4.8241	3.7660	2.8711
E_{da}	15.7403	9.3469	7.7705
E_{dc}	12.6942	7.7964	5.9425
V_{ss}	–5.8787	–5.1076	–4.4532
V_{xx}	5.0545	0.7172	0.2715
V_{xy}	7.3168	3.6286	2.9182
V_{pcsa}	0.8742	4.1592	4.0969
V_{pasc}	4.8020	3.4948	2.8601
V_{dapc}	4.1776	4.7535	4.1220
V_{dcpa}	0.0000	0.1638	0.2738

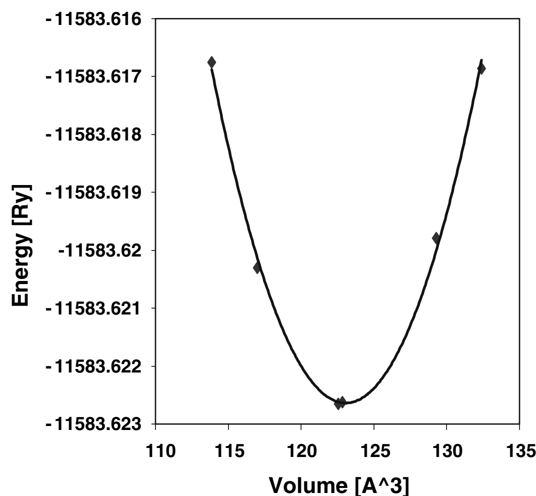

Fig. 1 Total energy of c-InN versus the lattice volume

is less than the value (5.03 Å) [63] of FP-LAPW by 1.25%. With respect to the lattice constant values (4.92 and 4.929 Å) of FP-LMTO [56, 62] our result is high by (0.8–0.95)%. The values of a calculated by PP [54, 60] are very close to our result; the discrepancy is about (0.06–0.32)%. But the discrepancy is 0.7% with respect to the corrected lattice constant value of another PP calculations [55].

At the second stage of the work, we have employed the FP-LAPW method within the frame work of the DFT to calculate the band structure of c-InN. Since, this work is planned to be extended the bowing parameter calculations of alloys correspond to InN in the near future, we have focused mainly on the energy gaps at high symmetry points. It is found that, the band gap of InN is direct in zinc-blende phase, furthermore, the variation of energy bands is in agreement with the results of previous reports [10, 11, 52, 57, 79]. The present band edge at Γ point is non parabolic as it was reported in these works. Since we are unaware of reports of experimental investigations of the electronic properties of c-InN, we couldn't compare the present band gap values with the experimental facts. But, the present band gap at Γ point (E_g^Γ) is found to be very small (–0.012 eV) with respect to the values given by first principles calculations [10, 11]. The similar negative direct band gap energies [55, 57, 61, 63] and small positive ones [52, 59] were reported before in the literature. In the present work, the calculated negative direct energy gap originated from DFT calculations has been adjusted to the value of 0.59 eV by addition of necessary energy corresponds to the effect which is not included in the calculations initially. The half of the energy difference between 0.59 eV and the present direct band gap is added to the conduction band and subtracted from the valence band state energies equally in the same manner defined in Ref. [80]. Similarly, the negative value of E_g^Γ in Ref. [52] and the small value of E_g^Γ in Ref. [10] have been corrected by inclusion of some external potentials and quasiparticle corrections, respectively. In the present work, the adjusted direct band gap value of 0.59 eV is taken from Ref. [10]. The same direct band gap value has been used in a very recent EPP calculations of InN [79]. The direct band gap value of 0.59 eV has been decided by the feedback calculations; the adjusted direct band gap of c-InN has been tested by electronic band structure calculations of c-$In_xGa_{1-x}N$ alloys. The direct band gap of $In_xGa_{1-x}N$ alloy is calculated to be 3.198, 3.065, 2.967 and 2.647 eV for the In concentrations of 0.03, 0.07, 0.10 and 0.20, respectively. These present direct band gap values of c-$In_xGa_{1-x}N$ alloys are found to be very close to the direct band gap values of 3.2, 3.1, 3.0 and 2.875 eV which are measured by PL spectra of c-$In_xGa_{1-x}N$ films for the same concentrations of In at 2 K [81]. In these feedback calculations, we have employed the ETB calculations and derived the corresponding energy parameters from the present eigenvalues of FP-LAPW with respect to the adjusted direct band gap of InN. The ETB energy parameters of GaN used in the present calculations have been obtained by the same calculational steps explained in the following paragraphs.

Since the present energy parameters of ETB in feedback calculations produce the experimental direct band gap energies of c-$In_xGa_{1-x}N$ alloys for different concentrations of In we have surely adjusted the direct band gap value of c-InN to 0.59 eV. The adjusted energy band structure of c-InN by FP-LAPW is shown in Fig. 2. Table 3 gives the important features of the present and previously reported band structures for c-InN at high symmetry points. The energy gaps at X and L (E_g^X), (E_g^L) which are enlarged to the values of 3.375 and 4.249 eV are in good agreement with the results reported in Refs. [10, 11, 23] and [10, 11], respectively.

Table 2 The theoretical and experimental lattice constant values (a_{th}, a_{exp}) in Å for InN, InAs and InSb in cubic phase

Compound	a_{th}	a_{exp}
InN	4.967[a], 4.95[b,c,d]	4.98[t], 4.97[u]
	(4.97, 5.05)[e]	4.986[w]
	4.932[f], 4.929[g]	
	4.953[h],(5.004,5.109)[i]	
	4.974[j], 5.01[k]	
	4.983[l], 5.06[m]	
	5.017[n], 4.92[o]	
	5.03[p] (4.964, 5.067)[r]	
	4.968[s]	
InAs	6.194[a], 5.906[b′], 5.85[c′]	6.058[e′], 6.036[f′]
	(6.063, 5.94)[d′]	6.06[g′]
InSb	6.643[a]	6.4782[h″], 6.47937[i″]
	6.34[b″], 6.36[c″]	6.49[j″]
	(6.34, 6.464)[d″]	
	6.42[e″], 6.478[f″]	

[a] Present work, [b] Ref. [52], [c] Ref. [10], [d] Ref. [53], [e] Ref. [54], [f] Ref. [55], [g] Ref. [56], [h] Ref. 20 in Ref. [55], [i] Ref. [57], [j] Ref. [58], [k] Ref. [59], [l] Ref. [60], [m] Ref. [61], [n] Ref. [11], [o] Ref. [62], [p] Ref. [63], [r] Ref. [64], [s] Ref. [65], [t] Ref. [66], [u] Ref. [5], [w] Ref. [8], [b′] Ref. [67], [c′] Ref. [68], [d′] Ref. [69], [e′] Ref. [70], [f′] Ref. [71], [g′] Ref. [72], [b″] Ref. [73], [c″] Ref. [67], [d″] Ref. [69], [e″] Ref. [74], [f″] Ref. [75], [h″] Ref. [76] [i″] Ref. [77], [j″] Ref. [78]

In the following step of the present work, the energy parameters of ETB have been derived for c-InN from the band structure of DFT (Fig. 2) by the fitting process explained in ''The electronic structure calculations'' section. The band structure of c-InN recalculated by ETB is shown

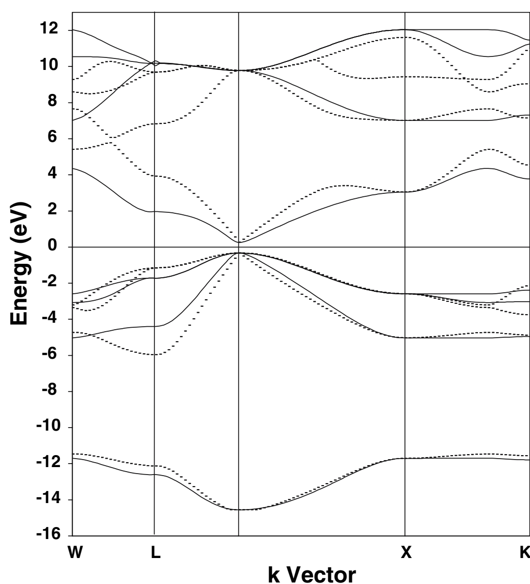

Fig. 2 The energy band structure of c-InN by FP-LAPW(adjusted) (*dotted line*) and ETB (*solid line*)

in Fig. 2. The imported features of the band structure at high symmetry points are listed in Table 3. In view of Fig. 2, we note that there is a close agreement between the band structure of c-InN by ETB and DFT at Γ and X points. Hence, the derived energy parameters of ETB can be used surely in the band structure calculations of c-InN and its alloys. The direct band gap of c-InN recalculated by ETB is exactly the same with the adjusted value of 0.59 eV in DFT calculations. The present direct gap of ETB is 20% smaller than the value of ab-initio self-consistent calculations in which the experimental lattice constant value (4.98 Å) of c-InN was used within LDA and the Bagayoko, Zhao, Williams (BZW) implementation of the linear combination of atomic orbitals [11]. The present E_g^{Γ} is only 9.2% smaller than the value of 0.65 eV calculated by the theoretical lattice constant of c-InN in the same report [11]. The present direct band gap value of c-InN is exactly the same with its corrected value reported in Ref. [10]. The present E_g^{Γ} of c-InN is approximately 16% smaller than the value calculated by DFT-LDA [55] and LDA based semi-empirical methods [82]. On the other hand, exactly the same energy gap at X point is obtained for c-InN by both ETB and DFT calculations. The present band gap values at X and L points are closer to the corresponding values given in Refs. [10, 11, 23] and [10, 11, 79], respectively. It is found that the present band gap energies of c-InN by ETB at high symmetry points (Γ, X, L) are in more agreement with the results of the calculations based on DFT within LDA-quasi particle corrections [10]. In the present ETB calculations, the valence band width is calculated to be 14.225 eV which is very close to the value of 14.179 eV calculated by DFT within LDA-BZW implementation [11]. The present valence band width of c-InN is also close to the value of 14.79 eV, although, the direct band gap value was calculated to be –0.48 eV in the same work [63].

InAs

In the present work, the equilibrium value of the lattice constant for InAs is determined by the total energy calculations based on DFT/GGA-FPLAPW. The total energy calculations are carried on a set of volumes and fitted to Murnaghan equation [51]. We have adopted the value of 1.2 Å for In and 1.15 Å for As as the MT radii. The electronic configuration of InAs is In:Kr ($4d^{10}5s^25p^1$) and As:Ar ($3d^{10}4s^24p^3$). In the calculations, the electrons of In in ($1s^22s^22p^63s^23p^63d^{10}4s^24p^64d^{10}$) are defined as the core electrons and distinguished from the valence electrons of In in ($5s^25p^1$). Similarly, the inner shell electrons of As in ($1s^22s^22p^63s^23p^63d^{10}$) are distinguished from the valence electrons of As in ($4s^24p^3$). The curve of the total energy versus the unitcell volume is shown in Fig. 3. The equilibrium lattice constant of InAs is calculated to be 6.194 Å.

Table 3 A summary of the important features, energy gaps and valance bandwidths of the present DFT (adjusted) and ETB band structure for c-InN compared to other experimental and theoretical calculational results

	DFT[a] (adjusted)	ETB[a]	Theoretical		
			LDA-BZW[b]	EPP[c]	DFT-LDF[d]
Γ_1^v	–14.557	–14.557	–14.179		
Γ_{15}^v	–0.332	–0.332	0.000	0.000	0.000
Γ_1^c	0.258	0.258	0.654	0.592	0.435
Γ_{15}^c	9.779	9.779	9.762	9.597	10.174
X_1^v	–11.704	–11.704	–11.309		
X_3^v	–5.031	–5.031	–4.750	–4.795	–4.687
X_5^v	–2.594	–2.594	–2.209	–1.481	–1.687
X_1^c	3.043	3.043	4.182	4.758	2.903
X_3^c	7.012	7.012	6.898	5.102	6.322
L_1^v	–12.127	–12.608	–11.762		
L_1^v	–5.969	–4.399	–5.571	–4.967	–5.229
L_3^v	–1.159	–1.718	–0.834	–0.460	–0.557
L_1^c	3.917	1.951	4.032	3.213	3.831
L_3^c	9.683	10.173	8.434	10.040	6.954
Γ_{15}^v–Γ_1^c	0.59	0.59	(0.738, 0.65)[b]	0.592[c]	0.592[d]
			0.70[e,f]		
Γ_{15}^v–X_1^c	3.375	3.375	4.182[b]	4.758[c]	2.903[d]
			2.51[e]		
Γ_{15}^v–L_1^c	4.249	3.670	4.032[b]	3.213[c]	3.831[d]
			5.82[e]		
Γ_1^v–Γ_{15}^v	14.225	14.225	14.179[b]	14.79[g]	

All energies are in eV

[a] Present work, [b] Ref. [11], [c] Ref. [79], [d] Ref. [10], [e] Ref. 20 in Ref. [55], [f] Ref. [82], [g] Ref. [63]

The present lattice constant of InAs is given in Table 2 together with the experimental and other calculated lattice constant values of InAs presented in the literature. In an early work [70], the lattice constant of InAs was measured to be 6.058 Å at room temperature. Another experimental lattice constant value of InAs was given as 6.036 Å in Ref. [71]. In a resent work [72], the value of 6.06 Å has been extracted from the reflectance difference spectra of the InAs grown on InP. The present lattice constant of InAs at 0 K is about 2.2–2.6% greater than these measured values at room temperature. The lattice constant values of both 5.906 and 5.94 Å have been calculated by ab-initio pseudo potentials [67, 69]. In another theoretical work, the lattice constant of InAs has been calculated as 5.85 Å by generalized density functional theory (GDFT) within LDA (GDFT/LDA) [68]. It is found that, the present equilibrium lattice constant value of 6.194 Å is in more agreement with the value of (6.063 Å) DFT/LDA-FPLAPW [69] than the values of ab-initio pseudopotential [67, 69] and GDFT/LDA calculations [68]. The difference is only 2.2%.

In the present work, the energy band structure of InAs has been calculated by DFT/GGA-FP-LAPW for the present equilibrium lattice constant value of InAs. We have concentrated mainly on the energy gaps at high symmetry points. It is found that, band gap of InAs is direct. The variation of energy bands is in agreement with the results of nonlocal PP calculations [27]. The present band structure of InAs is also very close to the band structure of ETB [32, 49] except along Γ–*X* direction. The band structure has a maximum point along Γ–*X* direction in both present and nonlocal PP calculations [27], but in ETB calculational results [32, 49] it approaches to *X* point constantly by passing through a point of inflection. In the present calculations, the energy values of the main features at high symmetry points (Γ_1^v, X_1^v, X_3^v, X_5^v, L_3^v) are in good agreement with the corresponding values measured by PL spectra [20]. But, the direct band gap of InAs (0.277 eV) is found to be smaller than its experimental values reported in Refs. [16, 19, 21–25]. The present narrow direct band gap of InAs has been adjusted to the value of 417 meV which is recommended in Ref. [83], with respect to the available experimental values. The half of the energy difference between 417 meV and the present direct band gap is added to the conduction and subtracted from the valence band state energies equally in the same manner defined in Ref. [80]. The adjusted energy band structure of InAs by

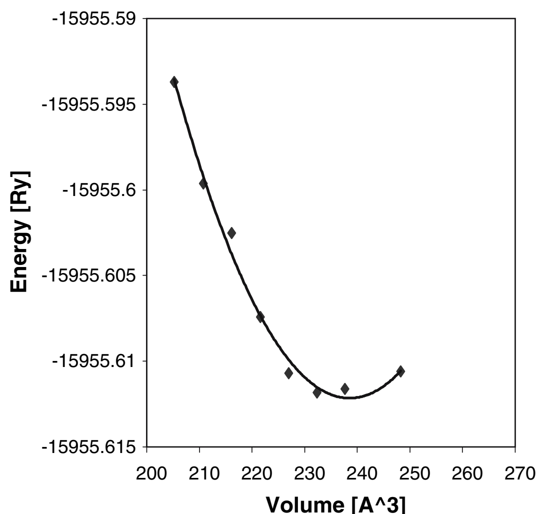

Fig. 3 Total energy of InAs versus the lattice volume

DFT/GGA-FP-LAPW is shown in Fig. 4. Table 4 gives the important features of the present and previously reported band structures for InAs at high symmetry points. The present energy gaps at X and L points are enlarged to 1.787 and 1.461 eV, respectively by adjustment.

In the following stage of the work, the energy parameters of ETB have been derived for InAs from the band structure of DFT (Fig. 4) by the fitting process explained in the ''The electronic structure calculations'' section. The recalculated band structure of InAs by ETB is shown in Fig. 4. The important features of the band structure at high symmetry points are listed in Table 4. As it is observed in Fig. 4, the valence band structure of InAs by ETB follows the that of DFT along both Γ–X and Γ–L directions closely. The variation of the first conduction band energy of InAs is similar in both ETB and DFT results along Γ–L direction. The first state energies of the conduction band by ETB deviate from the present results of DFT along Γ–X direction and approach to the X point constantly. The similar variation was plotted by ETB calculations for both sp^3s^* and $sp^3s^*d^5$ interactions of InAs in Refs. [49] and [32], respectively. The energy gaps of InAs at Γ and X points are found to be exactly the same by both present ETB and DFT calculations. The present E_g^Γ value of 0.417 eV is very close to the corresponding values of EPP [29] and ETB [30, 31] calculations. The present E_g^Γ is only 0.71% smaller than the value of 0.42 eV calculated by DFT within LDA [26]. The present direct band gap of InAs is about 12.7% greater than the value reported by both tight binding calculations within Green's functional approach [28] and nonlocal EPP calculations [27]. The present E_g^X is found to be 18% smaller than that of the ETB calculations based on $sp^3s^*d^5$ basis and spin-orbit interactions [31]. But the present E_g^X is still in the range (1.394–2.33 eV) of the values calculated by different methods [16, 26–29]. The E_g^L of present ETB calculations is found to be closer to the corresponding values given by empirical tight binding [28, 31] and EPP [27] calculations than the values of DFT-LDA [26] and EPP [29] calculations. The width of the valence band is found to be the same by both present ETB and DFT/GG-FP-LAPW calculations; it is about (4.77–13.55)% smaller than the values reported in Refs. [26–28, 31].

In the present work, the effective mass of the electrons and holes are calculated by least square fitting method by following the curvature of the corresponding band structure of InAs around Γ point. The calculated effective mass values of InAs are $0.0221m_0$, $0.4344m_0$, and $0.0283m_0$ for electrons, heavy and light holes, respectively. The present electron and light hole effective masses are very close to the corresponding experimental ($0.023m_0$, $0.026m_0$) and calculational values ($0.023m_0(0.02353m_0)$, $0.02811m_0$) reported in Ref. [23] and Refs. [32], respectively. But the present effective mass of the heavy holes at Γ point is found to be 24% greater than its experimental value of $0.35m_0$ [23].

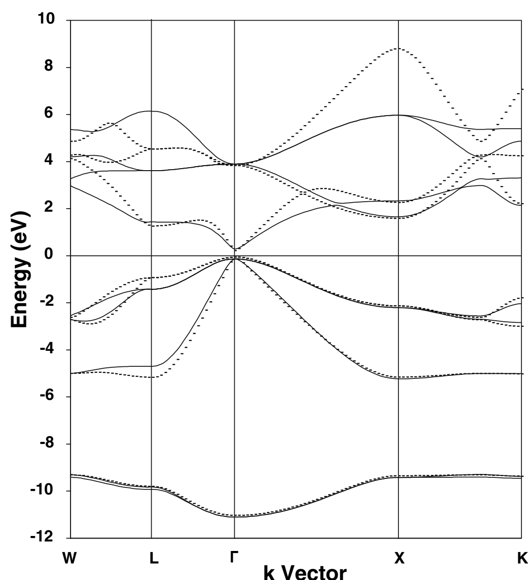

Fig. 4 The energy band structure of InAs by FP-LAPW(adjusted) (*dotted line*) and ETB (*solid line*)

InSb

The equilibrium lattice constant value of InSb is determined by total energy calculations based on DFT within GG approximation. The total energy for a set of volumes has been calculated by FP-LAPW method and fitted to the Murnaghan equation [51]. We have adopted the value of 1.058 Å for In and 1.058 Å for Sb as the MT radii. The electronic configuration of InSb is In:Kr ($4d^{10}5s^25p^1$) and Sb:Kr ($4d^{10}5s^25p^3$). In the calculations, the electrons of In

Table 4 A summary of the important features, energy gaps and valance bandwidths of the present DFT (adjusted) and ETB band structure for InAs compared to other experimental and theoretical calculational results

	DFT[a] (adjusted)	ETB[a]	Theoretical				Experimental
			DFT[b]	ETB[c]	EPP[d]	ETB[e]	PL[f]
Γ_1^v	–11.102	–11.102	–11.52	–12.69	–12.69	–12.188	–12.3
Γ_{15}^v	–0.132	–0.132	0.00	0.00	0.0	0.0	
Γ_1^c	0.285	0.285	0.42	0.37	0.37	0.418	
Γ_{15}^c	3.898	3.898	3.68	4.39	4.39	4.252	4.39[f′]
X_1^v	–9.419	–9.419	–9.39	–10.20	–10.20		–9.8
X_3^v	–5.230	–5.230	–6.16	–6.64	–6.64		–6.3
X_5^v	–2.205	–2.205	–2.41	–2.47	–2.47	–2.654	–2.4
X_1^c	1.655	1.655	2.33	2.28	2.28	2.176	
X_3^c	2.331	2.331	2.77	2.66	2.26		
L_1^v	–9.875	–9.924	–10.03	–10.99	–10.92		–10.6[f′]
L_1^v	–5.237	–5.237	–6.03	–6.87	–6.23		
L_3^v	–1.003	–1.418	–1.01	–1.05	–1.26	–1.124	–0.9
L_1^c	1.329	1.425	1.13	1.50	1.53	1.691	
L_3^c	4.601	3.614	5.20	5.84	5.42	4.723	
$\Gamma_{15}^v–\Gamma_1^c$	0.417	0.417	0.42[b] 0.419[i]	0.37[c,d]	0.418[g,e]	0.417[h]	0.418[j,k], 0.416[l,m] 0.420[n], 0.415[o]
$\Gamma_{15}^v–X_1^c$	1.787	1.787	2.33[b] 2.176[e]	2.28[c,d]	1.433[l]	1.398[i]	
$\Gamma_{15}^v–L_1^c$	1.461	1.587	1.13[b,k] 1.691[e]	1.50[c]	1.53[d]	1.110[i]	
$\Gamma_1^v–\Gamma_{15}^v$	10.970	10.970	11.52[b]	12.69[c,d]	12.188[e]		

All energies are in eV

[a] Present work, [b] Ref. [26], [c] Ref. [28], [d] Ref. [27], [e] Ref. [31], [f] Ref. [20], [f′] Ref. [23], [g] Ref. [30], [h] Ref. [83], [i] Ref. [29], [j] Ref. [23], [k] Ref. [20], [l] Ref. [16], [m] Ref. [21], [n] Ref. [24], [o] Ref. [25]

in ($1s^22s^22p^63s^23p^63d^{10}4s^24p^64d^{10}$) are defined as the core electrons and distinguished from the valence electrons of In in ($5s^25p^1$). Similarly, the inner shell electrons of Sb in ($1s^22s^22p^63s^23p^63d^{10}4s^24p^64d^{10}$) are distinguished from the valence band electrons of Sb in ($5s^25p^3$) shell. The total energy of InSb as a function of unit cell volume is shown in Fig. 5. The calculated total energy of InSb is found to be minimum with the lattice constant value of 6.643 Å. The present lattice constant of InSb is given in Table 2 together with the experimental and the other calculated lattice constant values of InSb presented in the literature. In a very early work [76], the lattice constant of InSb was measured as 6.4782 Å at room temperature by electron diffraction method. The similar experimental value (6.47937 Å) was given in Ref. [77]. Besides, the temperature dependence of the lattice constant of InSb was given also in Ref. [77] in the range of 10–60 °C. Another experimental lattice constant value of 6.49 Å was tabulated in Ref. [78] for InSb. The present lattice constant of InSb is about (2.3–2.5)% greater than these measured values. In the literature, the first theoretical lattice constant values for InSb were given by ab-initio pseudopotential calculations [67, 69, 73]; they were 6.36 and 6.34 Å, respectively. The present lattice constant value of InSb is about (4.4–4.7)% greater than these pseudopotential calculational results. The first full potential calculations for InSb was also studied by Massidda et al. [69]. They found that, the lattice constant of InSb by DFT/LDA-FP-LAPW calculations had better agreement with the experimental results than those of ab-initio pseudo potential calculations [67, 69, 73]. The following two lattice constant values (6.42 and 6.478 Å) in Table 2 were again calculated by full potential calculations [74, 75]. The present equilibrium lattice constant value of 6.643 Å is found to be about (2.5–3.4)% greater then these first principles calculational results [74, 75].

In the present work, the energy band structure of InSb has been calculated by DFT/GGA-FP-LAPW for the present lattice constant of InSb. In the present first principles calculations, the energy gap of InSb is found to be direct. The present order between the energy gaps, $E_g^{\Gamma} < E_g^{L} < E_g^{X}$, is the same as it was reported in all previous theoretical works [26–29, 32, 41–43, 74]. Besides, the variation of the bands is found to be similar with the results given in these works [26–29, 32, 41–43, 74]. In both present and

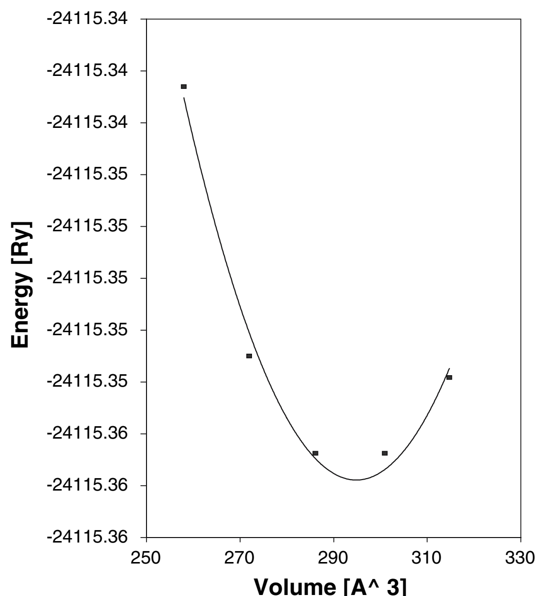

Fig. 5 Total energy of InSb versus the lattice volume

previously reported results [29, 41, 43, 74] the energy variation of the highest valance band and the lowest conduction band can be characterized by a very sharp slope at Γ point. The present energy of the first conduction band state has a maximum along Γ–*X* and Γ–*L* directions. This variation is exactly the same with the DFT/LDA-FP-LAPW results of Guo et al. [74]. But in the other calculations [29, 32, 41, 43], the energy of the first conduction band state approaches to *L* point with an approximately constant slope. In the present work, the E_g^Γ of InSb is found to be small (0.08 eV) as the uncorrected direct band gap values reported in the previous works [42, 43, 74]. The present semimetallic band structure of InSb at Γ point is corrected; the E_g^Γ is enlarged to its experimental value of 0.235 eV empirically as it is done for the band gap values of InN and InAs [19, 23, 38]. The ETB interaction parameters of $sp^3s^*d^5$ basis in Ref. [31] were also fitted to the experimental band gap value of 0.235 eV at Γ point. The adjusted energy band structure of InSb by DFT/GGA-FP-LAPW is shown in Fig. 6. Table 5 gives the important features of the present and previously reported band structures for InSb at high symmetry points. The enlarged energy gaps at *L* and *X* points are very close to the values of 0.82 and 1.55 eV, respectively which were calculated by DFT/LDA-FP-LAPW [43].

In the present work, we have employed a fitting process to obtain the ETB energy parameters of InSb from the present eigenvalues of DFT (Fig. 6). The recalculated band structure of InSb by ETB is shown in Fig. 6. The important features of the ETB band structure at high symmetry points are listed in Table 5. The valence band structure of InSb is found to be exactly the same by both present ETB and DFT calculations. The sharp and smooth variations of the band structure of InSb around Γ and *X* points, respectively have been produced successfully by the present ETB energy parameters. The energy gaps of InSb at Γ and *X* points are found to be exactly the same by both ETB and DFT calculations. The present E_g^Γ value of 0.235 eV is very close to the values calculated by EPP [29], DFT-LDA [26] and relativistic self-consistent LMTO scheme [42]. The present E_g^Γ is about (6–9.6)% smaller than the corresponding value calculated by nonlocal PP [27], tight binding Green's functional approach [28] and self-consistent PP [41]. The corrected band gap energy values reported in Refs. [43, 44] are about (12–30)% smaller than the present E_g^Γ. The calculated band gap at *X* point is very close to the value of 1.55 eV which was obtained by the corrected results of DFT/LDA calculations [43]. On the other hand, the present E_g^X is found to be 13% smaller than that of ETB calculations based on $sp^3s^*d^5$ basis interactions [31]. In their ETB calculations [31], the inclusion of all d orbital interactions as well as sp^3 and s^* and the determination of the lattice by the experimental lattice constant of InSb were all effective to obtain the available experimental energy gap of InSb at point *X* [25]. The present band gap value of InSb at point *L* is in the range (0.70–1.227) of values given in the literature [26–29, 31, 43, 44]. On the other hand, the width of the valence band is the same for both present ETB and DFT calculations, but it is about (13–22)% smaller than the available experimental [84, 85] and theoretical results [26–28, 31, 43, 74, 75].

In the present work, the effective mass of the electrons and holes of InSb are calculated at Γ point. The calculated effective mass values of InSb are $0.0152m_0$, $0.371m_0$, and

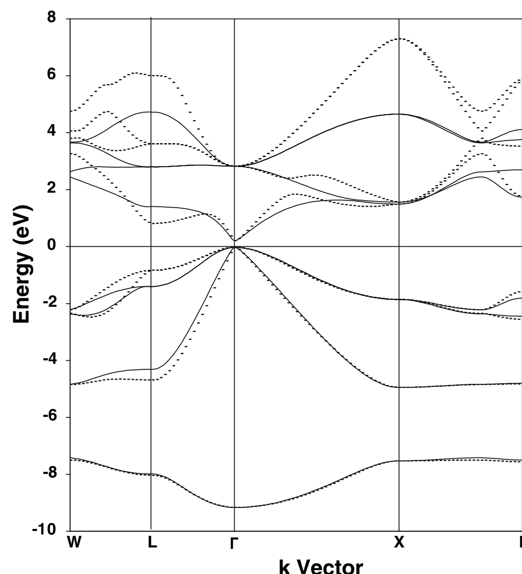

Fig. 6 The energy band structure of InSb by FP-LAPW(adjusted) (*dotted line*) and ETB (*solid line*)

Table 5 A summary of the important features, energy gaps and valance bandwidths of the present DFT (adjusted) and ETB band structure for InSb compared to other experimental and theoretical calculational results

	DFT[a] (adjusted)	ETB[a]	Theoretical				Experimental
			Non. PP[b]	DFT[c]	ETB[d]	ETB[e]	PL[f]
Γ_1^v	–9.167	–9.167	–11.71	–10.52	–11.71	–11.435	–11.71
Γ_{15}^v	–0.029	–0.029	0.00	0.00	0.0		
Γ_1^c	0.206	0.206	0.25	0.24	0.25		
Γ_{15}^c	2.822	2.822	3.16	2.66	3.16	3.503	3.37[f′]
X_1^v	–7.530	–7.530	–9.20	–8.54	–9.20		–9.0
X_3^v	–4.950	–4.950	–6.43	–5.84	–6.43		–6.4
X_5^v	–1.859	–1.859	–2.25	–2.52	–2.45	–2.722	–2.4
X_1^c	1.493	1.493	1.71	1.71	1.71	1.756	1.79[f′]
X_3^c	1.564	1.564	1.83	2.23	1.81		
L_1^v	–8.040	–7.986	–9.95	–9.13	–10.03		
L_1^v	–4.691	–4.315	–5.92	–5.79	–6.81		
L_3^v	–0.836	–1.398	–1.44	–1.08	–1.06	–1.30	–1.05, –1.4[f′]
L_1^c	0.810	1.401	1.03	0.70	0.99	1.227	
L_3^c	3.608	2.799	4.30	4.13	5.46	4.059	
Γ_{15}^v–Γ_1^c	0.235	0.235	0.25[b,d]	0.24[c,g]	0.2351[h]	0.18[i]	0.235[l,m,n], 0.2352[o]
			0.21[j]	0.26[k]		0.235[e]	0.24[p], 0.18[r], 0.23[s]
Γ_{15}^v–X_1^c	1.522	1.522	1.71[b,c,d]	0.6618[h]	1.55[i]	1.82[j] 1.756[e]	1.79[p]
Γ_{15}^v–L_1^c	0.839	1.430	1.03[b]	0.70[c]	0.99[d]		
			0.9743[h]	0.82[i]	1.02[j]	1.227[e]	
Γ_1^v–Γ_{15}^v	9.138	9.138	11.71[b,d]	10.52[c]	11.57[i]		11.7[w]
			10.9[t]	(10.83, 11.05)[u]	11.435[e]		11.2[x]

All energies are in eV

[a] Present work, [b] Ref. [27], [c] Ref. [26], [d] Ref. [28], [e] Ref. [31], [f] Ref. [20], [f′] Ref. [23], [g] Ref. [42], [h] Ref. [29], [i] Ref. [43], [j] Ref. [44], [k] Ref. [41], [l] Ref. [19], [m] Ref. [38], [n] Ref. [23], [o] Ref. [39], [p] Ref. [25], [r] Ref. [40], [s] Ref. [37], [t] Ref. [74], [u] Ref. [75], [w] Ref. [84], [x] Ref. [85]

$0.028m_0$ for electrons, heavy and light holes, respectively. The present electron, heavy and light hole effective masses are very close to the corresponding experimental ($0.0136m_0$, $0.34m_0$ and $0.0158m_0$) values reported in Ref. [23].

Conclusion

In the present work, the electronic band structure of InN, InAs and InSb has been investigated by ETB method. The energy parameters of ETB for sp^3d^2 basis and nearest neighbor interactions have been derived from the eigenvalues of the present DFT/GGA-FP-LAPW calculations carried on InN, InAs and InSb compounds. Since the band gap values of the compounds are responsible for the band gap engineering of their ternary and quaternary alloys, we have concentrated to have well defined band gaps for InN, InAs and InSb at high symmetry points especially at Γ point. The present DFT/GGA-FP-LAPW calculations show that InN, InAs and InSb have direct band gap structures in zinc-blende phase. The band structure of the compounds is found to be similar with the calculational results reported in the literature. However, the band gap values of the compounds are found to be small with respect to the corresponding available experimental data. In the present work, the direct band gap values of FP-LAPW/GGA calculations have been adjusted to the available experimental gaps for both InAs and InSb compounds. Since we are unaware of reports of experimental investigations of the electronic properties of c-InN, we have adjusted the direct band gap of it to the corrected value given in the literature by DFT-LDA calculations. In the present total energy calculations for volume optimization, the lattice constant of InAs and InSb has been calculated by about 2% discrepancy with respect to the corresponding experimental values. In the same calculations, we have obtained an excellent agreement between the present calculated and available experimental lattice constant values of InN.

The ETB energy parameters obtained from the present first principles calculations have been tested by recalculating the energy band structure of the compounds. It is found that, the ETB energy parameters can reproduce the valence band structure of InN, InAs and InSb satisfactorily.

The ETB valence band structure of compounds follows the valence band structure of DFT/GGA-FP-LAPW closely. The valence band width of the compounds is exactly the same for both present ETB and DFT calculations. The energy variation of the first conduction band state of the compounds does not follow the corresponding energy variation of the present DFT calculations closely, along Γ–X and Γ–L directions, like in all PP and ETB results. However, the ETB energy band gap values of the compounds are exactly the same with those of DFT/GGA-FP-LAPW at Γ and X points. Furthermore, the present ETB parameters of InAs and InSb obtained from DFT calculational results give reasonable effective electron and hole masses by reproducing the curvature of the band structure of the compounds correctly around Γ point. The present E_g^L of ETB is also very close to that of DFT for InAs. But for the other compounds, InN and InSb, the ETB energy parameters seem to be insufficient to give the present energy gap of DFT at L point. Although the present ETB parameters of sp^3d^2 give exactly the same E_g^X of the present DFT calculations, they are not normally as strong as the ETB parameters of $sp^3s^*d^5$ to give the available experimental band gap value of InSb at X point. Since all the compounds considered in this work are direct band gap structures, we can conclude that the present ETB energy parameters of minimal sp^3d^2 basis are reliable and consume the computational time for the fundamental band gap engineering calculations of ternary and quaternary alloys of InN, InAs and InSb with respect to total concentration range of the constituents.

References

1. Mohammad SN, Morkoç H (1996) Prog Quantum Electron 20:361
2. Yamamoto A, Tsujino M, Ohkubo M, Hashimoto A (1994) Sol Energy Mater Sol Cells 35:53
3. Wu J, Walukiewicz W, Yu KM, Ager JW III, Haller EE, Lu H, Schaff WJ, Saito Y, Nanishi Y (2002) Appl Phys Lett 80:3967
4. Matsuka T, Ohamoto H, Nakao M, Harima H, Kurimoto E (2002) Appl Phys Lett 81:1246
5. Tabata A, Lima AP, Teles LK, Scolfaro LMR, Leite JR, Lemos V, Schöttker B, Frey T, Schikora D, Lischka K (1999) Appl Phys Lett 74:362; Lima AP, Tabata A, Leite JR, Kaiser S, Schikora D, Schöttker B, Frey T, As DJ, Lischka K (1999) J Crystal Growth 202:396
6. Kaczmarczyk G, Kaschner A, Reich S, Hoffmann A, Thomasen C, As DJ, Lima AP, Schikora D, Lischka K, Averbeck R, Riechert H (2000) Appl Phys Lett 76:2122
7. Lemos V, Silveira E, Leite JR, Tabata A, Trentin R, Scolfaro LMR, Frey T, As DJ, Schikora D, Lischka K (2000) Phys Rev Lett 84:3666
8. Cimalla V, Pezoldt J, Ecke G, Kosiba R, Ambacher O, Spieb L, Teichert G, Lu H, Schaff WJ (2003) Appl Phys Lett 83:3468
9. Guo Q, Yoshida A (1994) Jpn J Appl Phys Part 1 (33):2453
10. Bechstedt F, Furthmüler J (2002) J Crystal Growth 246:315
11. Bagayoko D, Franklin L, Zhao GL (2004) J Appl Phys 96:4297
12. Casey HC, Panish MB (1978) Heterostructure lasers. Academic, New York, and references therein
13. Luo LF, Beresford R, Wang WI (1998) Appl Phys Lett 53:2320
14. Bolognesi CR, Dvorak MW, Chow DH (1998) J Vac Sci Technol A 16:843
15. Fisher M, Krier A (1997) Infrared Phys Technol 38:405
16. Grober RD, Drew HD, Chyi J, Kalem S, Morkoc H (1989) J Appl Phys 65:4079
17. Marcadet X, Rakouska A, Prevot J, Glastre G, Vinter B, Erger V (2001) J Crystal Growth 227:609
18. Kim GH, Choi JB, Leem JY, Leem JY, Lee JI, Noh SK, Kim JS, Kang SK, Ban SI (2002) J Crystal Growth 234:110
19. Fang ZM, Ma KY, Jaw DH, Cohen RM, Stringfellow GB (1990) J Appl Phys 67:7034
20. Ley L, Pollak RA, McFeely FR, Kowalczyk SP, Shirley DA (1974) Phys Rev B 9:600
21. Fang ZM, Ma KY, Cohen RM, Stringfellow GB (1991) Appl Phys Lett 59:1446
22. Lacroix Y, Tran CA, Watkins SP, Thewalt MLW (1996) J Appl Phys 80:6416
23. Madelung O (ed) (1996) Semiconductors—basic data. Springer, Berlin, ISBN 3-540-60883-4
24. Dixon JR, Ellis JM (1961) Phys Rev 123:1560
25. Harrison WA (1980) Electronic structure and the properties of solids. Freeman, San Fransisco
26. Huang M, Ching WY (1985) J Phys Chem Solids 46:977
27. Chelikowsky JR, Cohen ML (1976) Phys Rev B 14:556
28. Talwar DN, Ting CS (1982) Phys Rev B 25:2660
29. Bouarissa N, Aourag H (1997) Infrared Phys Technol 38:153
30. Loehr JP, Talwar DN (1997) Phys Rev B 55:4353
31. Jancu J-M, Bassani F, Sala FD, Scholz R (1998) Phys Rev B 81:4838
32. Boykin TB, Klimeck G, Bowen RC, Oyafuso F (2002) Phys Rev B 66:125207
33. Theodorou G, Tsegas G (2000) Phys Rev B 61:10782
34. Volin CE, Garcia JP, Dereniak EL, Descour MK, Hamilton T, McMillan R (2001) Appl Opt 40:4501
35. Kirby BJ, Hanson RK (2002) Appl Opt 41:1190
36. Mishima TD, Santos MB (2004) J Vac Sci Technol B 22:1472
37. Dixit VK, Banial B, Venkataraman V, Bhat HL, Subbanna GN, Chandrasekharan KS, Arora BM (2002) Appl Phys Lett 80:2102
38. Rowell NL (1988) Infrared Phys Technol 28:37
39. Littler CL, Seiler DG (1985) Appl Phys Lett 46:986
40. Veal TD, Mahboob I, McConville CF (2004) Phys Rev Lett 92:136801
41. Mele EJ, Joannopoulos JD (1981) Phys Rev B 24:3145
42. Alouani M, Brey L, Christensen NE (1988) Phys Rev B 37:1167
43. Asahi R, Mannstadt W, Freeman AJ (1999) Phys Rev B 59:7486
44. Seidl A, Görling A, Vogl P, Majewski JA, Levy M (1996) Phys Rev B 53:3764
45. Blaha P, Schwarz K, Madsen GKH, Kvasnicka D, Luitz J (2001) WIEN2K, An augmented-plane-wave + local orbitals program for calculating crystal properties, Karlheinz Schwarz, Techn. Wien, Austria, ISBN 3-9501031-1-2
46. Perdew JP, Wang Y (1992) Phys Rev B 45:13244
47. Slater JC, Koster GF (1954) Phys Rev 94:1498
48. Harrison WA (1999) Elementary Electronic structure. World Scientific Publishing
49. Vogl P, Hjalmarson HP, Dow JD (1983) J Phys Chem Solids 44:365
50. Richardson SL, Cohen ML (1987) Phys Rev B 35:1388
51. Murnaghan FD (1944) Proc Natl Acad Sci USA 30:244
52. Christensen NE, Gorczyca I (1994) Phys Rev B 50:4397
53. Fuchs M, DaSilva JLF, Stampfl C, Neugebauer J, Scheffler M (2002) Phys Rev B 65:245212

54. Vogel D, Krüger P, Pollmann J (1997) Phys Rev B 55:12836
55. Wright AF, Nelson JS (1995) Phys Rev B 51:7866
56. Muñoz A, Kunc K (1993) J Phys Condens Matter 5:6015
57. Stampfl C, Van de Walle CG (1999) Phys Rev B 59:5521
58. Satta A, Fiorentini V, Bosin A, Meloni F, Vanderbilt D (1996) In: Dupuis RD, Edmond JA, Ponce F, Nakamura S (eds) Gallium nitride and related compounds. MRS symposia proceedings, no. 395. Materials Research Society, Pittsburgh, p 515
59. Nardelli MB, Rapcewicz K, Briggs EL, Bungaro C, Bernholc J (1997) In: Ponce FA, Moustakas TD, Akasaki I, Monemar BA (eds) III–V nitrides. MRS symposia proceedings no. 449. Materials Research Society, Pittsburgh, p 893
60. Yeh C-Y, Lu ZW, Froyen S, Zunger A (1992) Phys Rev B 46:10086
61. Van Schilfgaarde M, Sher A, Chen A-B (1997) J Crystal Growth 178:8
62. Kim K, Lambrecht WRL, Segall B (1996) Phys Rev B 53:16310
63. Ramos LE, Teles LK, Scolfaro LMR, Castineira JLP, Rosa AL, Leite JR (2001) Phys Rev B 63:165210
64. Zoroddu A, Bernardini F, Ruggerone P, Fiorentini V (2001) Phys Rev B 64:045208
65. Serrano J, Rubio A, Hernández E, Muñoz A, Mujica A (2000) Phys Rev B 62:16612
66. Chandrasekhar D, Smith DJ, Strite S, Lin M, Morkoç H (1995) J Crystal Growth 152:135
67. Zhang SB, Cohen ML (1987) Phys Rev B 35:7604
68. Remediakis IN, Kaxiras E (1999) Phys Rev B 59:5536
69. Massidda S, Continenza A, Freeman AJ, Pascale de TM, Meloni F, Serra M (1990) Phys Rev B 41:12079
70. Ozolin'sh JV, Averkieva GK, Ilvin'sh AF, Goryunova NA (1963) Sov Phys Cryst 7:691
71. Wyckoff RWG (1963) Crystal structures. Wiley, New York
72. Lin CH, Sun Y, Visbeck SB, Law DC, Hicks RF (2002) Appl Phys Lett 81:3939
73. Singh D, Varshni YP (1985) Phys Rev B 32:6610
74. Guo GY, Crain J, Blaha P, Temmerman WM (1993) Phys Rev B 47:4841
75. der Kellen SB, Freeman AJ (1996) Phys RevB 54:11187
76. Semiletov SA, Rozsibal M (1957) Kristallografiya 2:287
77. Straumanis ME, Kim CD (1965) J Appl Phys36:3822
78. Madelung O (ed) (1984) Numerical data and functional relationship in science and technology, Crystal and solid state physics, Vol. 17a, Landolt Börnstein. Springer, Berlin
79. Fritsch D, Schmidt H, Grundmann M (2004) Phys Rev B 69:165204
80. Godby RW, Schlüter M, Sham LJ (1988) Phys Rev B 37:10159
81. As DA, Schikora D, Lischka K (2003) Phys Stat Sol (c) 6:1607
82. Wei SH, Nie X, Batyrev IG, Zhang SB (2003) Phys Rev B 67:165209
83. Vurgaftman I, Meyer JR, Ram-Mohan L (2001) J Appl Phys 89:5815
84. Goldman A, Koch EE (eds) (1989) Numerical data and functional relationship in science and technology, New series, group III, Vol 23a. Springer, Berlin
85. Eastman DE, Grobman WD, Freeouf JL, Erbudak M (1974) Phys Rev B 9:3473